Near-field infrared spectroscopy of single layer $MnPS_3$

Sabine N. Neal,[†] Heung-Sik Kim,[‡] Kevin A. Smith,[†] Amanda V. Haglund,[¶] David G. Mandrus,[¶] Hans A. Bechtel,[§] G. Lawrence Carr,[‖] Kristjan Haule,[‡] David H. Vanderbilt,[‡] and Janice L. Musfeldt*[,†,⊥]

†*Department of Chemistry, University of Tennessee, Knoxville, Tennessee 37996, USA*

‡*Department of Physics and Astronomy, Rutgers University, Piscataway, New Jersey 08854, USA*

¶*Department of Materials Science and Engineering, University of Tennessee, Knoxville, Tennessee 37996, USA*

§*Advanced Light Source Division, Lawrence Berkeley National Laboratory, Berkeley, California 94720, USA*

‖*National Synchrotron Light Source II, Brookhaven National Laboratory, Upton, New York 11973, USA*

⊥*Department of Physics and Astronomy, University of Tennessee, Knoxville, Tennessee 37996, USA*

E-mail: musfeldt@utk.edu

Abstract

In order to explore the properties of a complex van der Waals material under confinement, we measured the near-field infrared response of the magnetic chalcogenide $MnPS_3$ in bulk, few-, and single-layer form and compared the results with traditional far field vibrational spectroscopy and complementary lattice dynamics calculations. Trends in the activated B_u mode near 450 cm^{-1} are particularly striking, with the disappearance of this structure in the thinnest sheets. Combined with the amplified response of the A_g mode and analysis of the $A_u + B_u$ features, we find that symmetry is unexpectedly *increased* in single-sheet $MnPS_3$. The monoclinicity of this system is therefore a consequence of the long-range stacking pattern rather than local structure.

Table of contents entry:

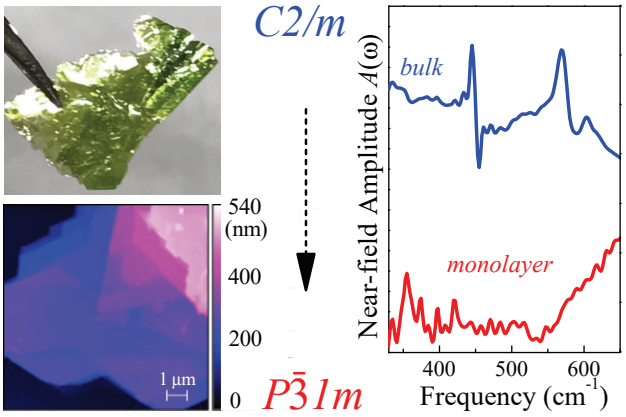

Keywords: near-field infrared spectroscopy, magnetic chalcogenide, $MnPS_3$, atomically-thin layer, symmetry analysis

Introduction

The layered structures of many chalcogenides allow for exfoliation, providing a unique platform for combining the complexity of bulk materials with the tunability of few- and single-layer systems.[1] One of the most widely investigated van der Waals materials is MoS_2.[2–5] Major findings include the indirect $\rightarrow$ direct gap crossover at the single layer level,[3,4] valley splitting effects driven by spin-orbit coupling,[6,7] and the confinement and symmetry-breaking effects that lead to unique chemical, electronic, optical, and thermal properties.[8–11] Complex chalcogenides are also attracting attention.[8,12] One of the most interesting initiatives involves the creation of robust, single-layer magnetic semiconductors like CrI_3, $CrSiTe_3$, and $MnPS_3$.[13–16] One commonality between all of these systems - from MoS_2 to $MnPS_3$ - is the role of Raman scattering to assure sample quality, probe even-symmetry vibrational modes, and explore confinement effects in the single layer.[5,17,18] The *ungerade* modes are, however, completely unexplored in few layer systems. Infrared spectroscopy is well suited for examining the fundamental excitations of the lattice, and because the technique probes odd-symmetry vibrations, it is useful for uncovering ferroelectric, vibronic, and spin-lattice coupling mechanisms.[19–22] Although it is highly desirable to extend toward few- and single-layer systems, traditional infrared spectroscopy cannot beat the diffraction limit for small sized (exfoliated) samples.[23]

Synchrotron-based infrared nanospectroscopy offers a path forward. The technique combines a high brightness, broadband synchrotron light source[24] with Fourier transform techniques and a tip-enhanced approach to enable spectroscopic work on small-sized samples and materials with micro- and nano-scale texture.[23,25–27] The spatial resolution, achieved by focusing infrared light onto an atomic force microscope (AFM) tip [Fig. 1(c)], is on the order of 20×20 nm^2. Initially, this technique was confined to the middle infrared[23] and proved powerful for exploring polaritons in graphene, unveiling the inhomogeneous character of the phase transition in VO_2, and studying heterogeneity in Bi_2Se_3 and Sb_2Se_3 nanocrystals.[28–31] Recently, the operational window has been expanded into the far infrared - down to 330

cm^{-1}.[25] Near-field infrared spectroscopy is therefore inviting new approaches to studying chalcogenides. This is because many (but not all) of the characteristic vibrational modes of these materials resonate in this frequency window. What distinguishes synchrotron-based near-field spectroscopy from tip-enhanced Raman scattering is the ability to explore odd- (rather than even-) symmetry vibration modes.[32]

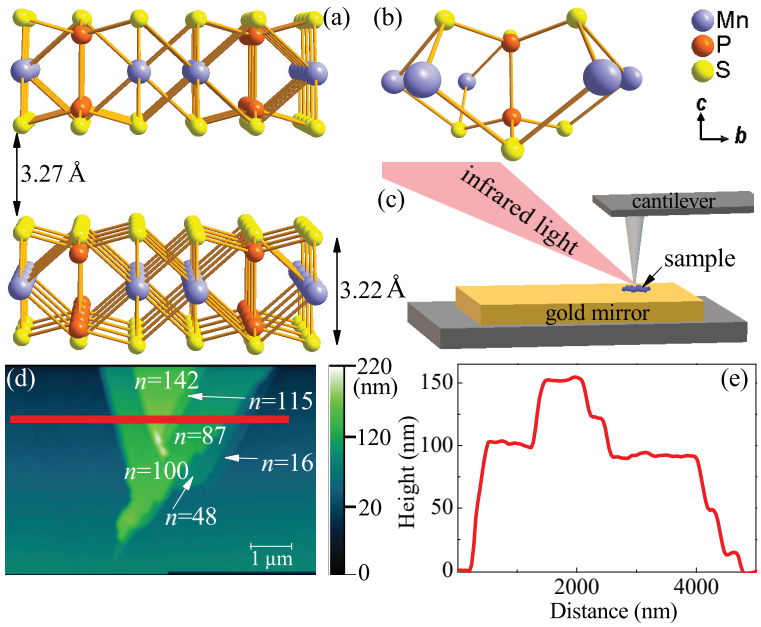

Figure 1: *(a) Crystal structure of monoclinic $MnPS_3$ showing the slab thickness and inter-layer distance. (b) Local structure for monolayer $MnPS_3$ emphasizing the bonding around the Mn center and the P-P dimer.*[33] *(c) Close-up schematic of the near-field setup showing the cantilever tip directing light to focus on a small area of the sample. Spatial resolution is on the order of 20 × 20 nm^2. (d) High resolution AFM image along with the corresponding layer number, extracted from (e) the height profile analysis along the red line in (d).*

We selected $MnPS_3$ as a platform with which to examine these ideas. This compound belongs to a large family of metal phosphorus trichalcogenides with the formula MPX_3 where M=metal ion, in this case high spin Mn^{2+} (S=$\frac{5}{2}$), and X=chalcogenide. This system is a non-collinear antiferromagnet below $T_N = 78$ K. It is also ferrotoroidic.[34] MPX_3 compounds can be viewed as salts of the phosphate anion, with Mn^{2+} cations and $(P_2S_6)^{4-}$ anions. These cations are linked together by Mn-X bonds, which are weaker than the bonds in the anion unit. This allows for a conceptual division of vibrational features into internal modes of the anion unit and external modes from the interactions between cation and anion.[35] Figure 1(a) shows the stacking of $MnPS_3$ into a monoclinic van der Waals solid.[33] The individual layer thickness is ≈ 3.22 Å, with each layer separated by a van der Waals gap of ≈ 3.27 Å. The local structure [Fig. 1(b)] is especially sensitive to symmetry. Rather than *C2/m*

like the bulk, the monolayer is proposed to be $P\bar{3}1m$ - assuming that the internal structure remains intact.[36] At this time, the possibility is untested. While extensive investigation of Raman scattering and light emission reveals strong electron-phonon coupling,[5,37] the infrared response of this system in few layer form is wholly unexplored. Because the behavior of *ungerade* vibrational modes is crucial for uncovering local structure modifications, testing various subgroup candidates, and developing higher-level functionalities like ferroelectricity,[19,38–40] bringing infrared spectroscopy to the field of few- and single-layer chalcogenides is an important step forward.

In order to explore odd-symmetry vibrational modes in few- and single-layer complex chalcogenides, we measured the near-field infrared response of $MnPS_3$ and compared our findings to first principles calculations. We find that features in the near-field spectrum of the single crystal are a combination of both infrared- and Raman-active modes. This mixed activation is a consequence of the tip-based nature of the technique. Detailed analysis of the near-field spectra supports a sized-induced symmetry crossover. The behavior of the B_u mode is most revealing. It is amplified in the n = 142 - 48 range but disappears below n = 11, indicative of a symmetry *increase* in few-sheet samples. Here, n is the layer number. Thus, single layer $MnPS_3$ is actually higher symmetry than previously supposed. This is interesting because local and long-range symmetry determine functionality in a variety of materials.

Results and discussion

Figure 2 summarizes the vibrational properties of single crystalline $MnPS_3$. In addition to the traditional infrared absorption, Raman scattering, and the theoretically-predicted mode positions, it also displays our near-field results. Combined with prior literature[41] and lattice dynamics calculations, we can assign all of the peaks in these spectra. Focusing first on the conventional infrared and Raman response, we assign the strong infrared band at 573

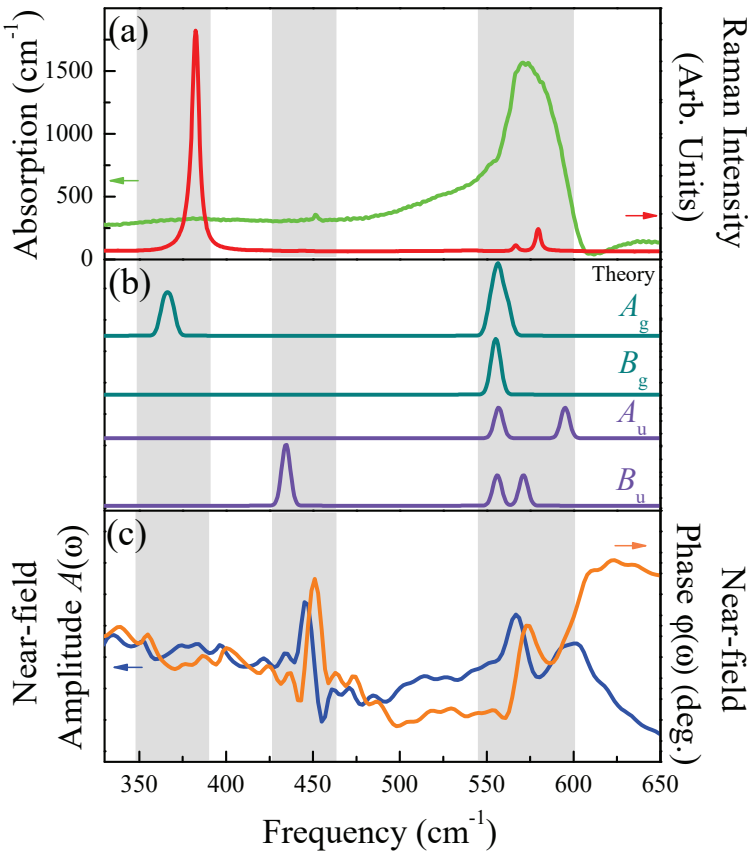

Figure 2: *(a) Traditional infrared absorption (green) and Raman scattering (red) spectra at 300 K. (b) Lattice dynamics calculations of $MnPS_3$ projected according to mode symmetry. Recall that the ungerade modes are infrared-active, and the gerade symmetry modes are Raman-active. The calculated frequencies are within 3% of the experimental peak positions. The calculated modes are shown with a Gaussian line shape and 2 cm^{-1} broadening. The higher peak intensity indicates near degeneracy. (c) Room temperature near-field amplitude (blue) and phase (orange) spectra for single crystalline $MnPS_3$. We set the overall frequency scale to focus on the available near-field energy window.*

cm^{-1} to the nearly degenerate PS_3 stretching mode. The presence of two weak Raman bands at 569 and 581 cm^{-1} shows that coupling between two PS_3 units is weak. The small infrared-active B_u mode at 452 cm^{-1} is a combination of a P-P stretch + out-of-plane PS_3 translation. The strongest Raman band near 385 cm^{-1} is due to a symmetric stretch of PS_3, largely ascribed to the motion of chalcogen atoms with a weak contribution from vibrational coupling between the phosporus and sulfur units.[41] As expected, the Mn-containing modes appear at lower frequencies. They are not included here in order to focus on the currently available frequency window.[25] Our assignments are summarized in Table 1.

Figure 2(c) displays the near-field spectrum of single crystalline $MnPS_3$ - both amplitude and phase - prior to exfoliation. Assignments are made by comparison with the aforementioned infrared and Raman spectroscopies as well as our calculated mode frequencies and displacement patterns. Clearly, the infrared-active modes are well represented in terms of position, shape, and amplitude confirming the effectiveness of the near-field technique. For

instance, the $A_u + B_u$ modes centered near 573 cm^{-1} are present in both sets of spectra, with the much smaller B_u mode increasing in intensity in the near-field response. At the same time, there are additional features that are not anticipated according to traditional selection rules. For instance, there is a subtle hint of the 360 cm^{-1} mode in the near-field spectrum that is likely an activated A_g mode - normally present in the Raman response. We therefore see that tip-enhanced infrared spectroscopy does not fully conform to traditional selection rules. This is because of tip curvature, the shape of the electric field lines, and penetration depth differences of the tip-enhanced technique.[42] Taken together, these assignments place near-field infrared spectroscopy of $MnPS_3$ on a firm foundation from which we can extend toward few- and single-layer systems.

Table 1: Vibrational mode assignments of single crystalline $MnPS_3$. All values are in cm^{-1}

ω (**infrared**)	ω (**Raman**)	ω (**near-field**)*	**assignment**
–	385	355	$\nu(PS_3)$
452	–	450	$T'_z(PS_3)$ + ν(P-P)
573	–	567	$\nu(PS_3)$
–	569, 581	–	$\nu(PS_3)$

ν = symmetric stretch, T' = translational motion, * Corresponds to maxima in the phase spectra.

As part of this work to measure few- and single-layer $MnPS_3$, we tested a variety of substrates for suitability with our target material. These included gold, aluminum, glass, sapphire, and silicon. The choice turns out to be crucial.[43] Our work with uncoated gold mirrors revealed excellent adhesion of few- and single-sheet $MnPS_3$ via gold$\cdots$surfur interactions. This not only eliminates the need for glue but also the interference of substrate phonons. The use of bare gold mirrors to support exfoliated chalcogenides does, however, have the disadvantage of introducing a small charge transfer band between the sulfur and the gold centered at 550 cm^{-1}.[44] This charge transfer excitation is somewhat problematic for $MnPS_3$ because it partially obscures some of the sulfur-related stretching modes between 550 and 600 cm^{-1}. We anticipate that uncoated gold will, however, work well for some of the heavier chalcogenides like $MoTe_2$ where the frequencies are shifted downward due to

heavier masses.[45] In any case, the charge transfer band is apparent only in the single-layer response for $MnPS_3$. We attempted to uncover the hidden $A_u + B_u$ phonon by modeling this Au$\cdots$S charge transfer with a series of Voigt oscillators and subtracting the result from the near-field spectrum. This procedure did not, unfortunately, reveal the superimposed phonons - probably due to their small oscillator strength. This limits the frequency window for single-layer $MnPS_3$ - although bilayer and above is relatively unaffected.

Turning our attention back to the magnetic chalcogenide, Fig. 3 summarizes the near-field infrared response of $MnPS_3$ at various layer thicknesses. The spectra and theoretically-predicted phonon pattern of the bulk crystal and monolayer in Fig. 3(a) reveal a stunning dissimilarity. Figure 3(b, c) shows a more systematic view of the near-field infrared response of $MnPS_3$ as a function of layer number (n). The gold$\cdots$sulfur interaction is particularly apparent in the single layer (n=1) spectrum as evidenced by the charge transfer band above 550 cm^{-1}.[44] The symmetry relationship between *C2/m* and $P\bar{3}1m$ is summarized in Fig 3(d). Remarkably, the vibrational response demonstrates that $MnPS_3$ single crystal has lower symmetry than few- and single-sheet analogs.

Detailed analysis of the near-field spectra [Fig. 3(b,c)] supports a size-induced symmetry crossover. The behavior of the B_u feature at 450 cm^{-1} is most revealing. This structure is relatively modest in the bulk (n=∞), increases slightly in intensity and blueshifts at intermediate sheet thicknesses, diminishes again, and disappears entirely below n=11. It never reappears - even at the monolayer - indicating that the symmetry for n <11 is no longer *C2/m*. Further, the symmetry must be *higher*, not lower, for this feature to disappear. To clarify the nature of the disappearance of the 450 cm^{-1} peak, calculated phonon frequencies from two separate single-layer structures with monoclinic and hexagonal symmetry constraints are shown in Fig 3(d). Note that the modes around 450 cm^{-1}, which exist in the monoclinic symmetry, are absent in the hexagonal case, indicating this feature is indeed linked to the restoration of three-fold symmetry in the single-layer limit.

The A_g mode near 376 cm^{-1} provides additional evidence for a change in symmetry. This

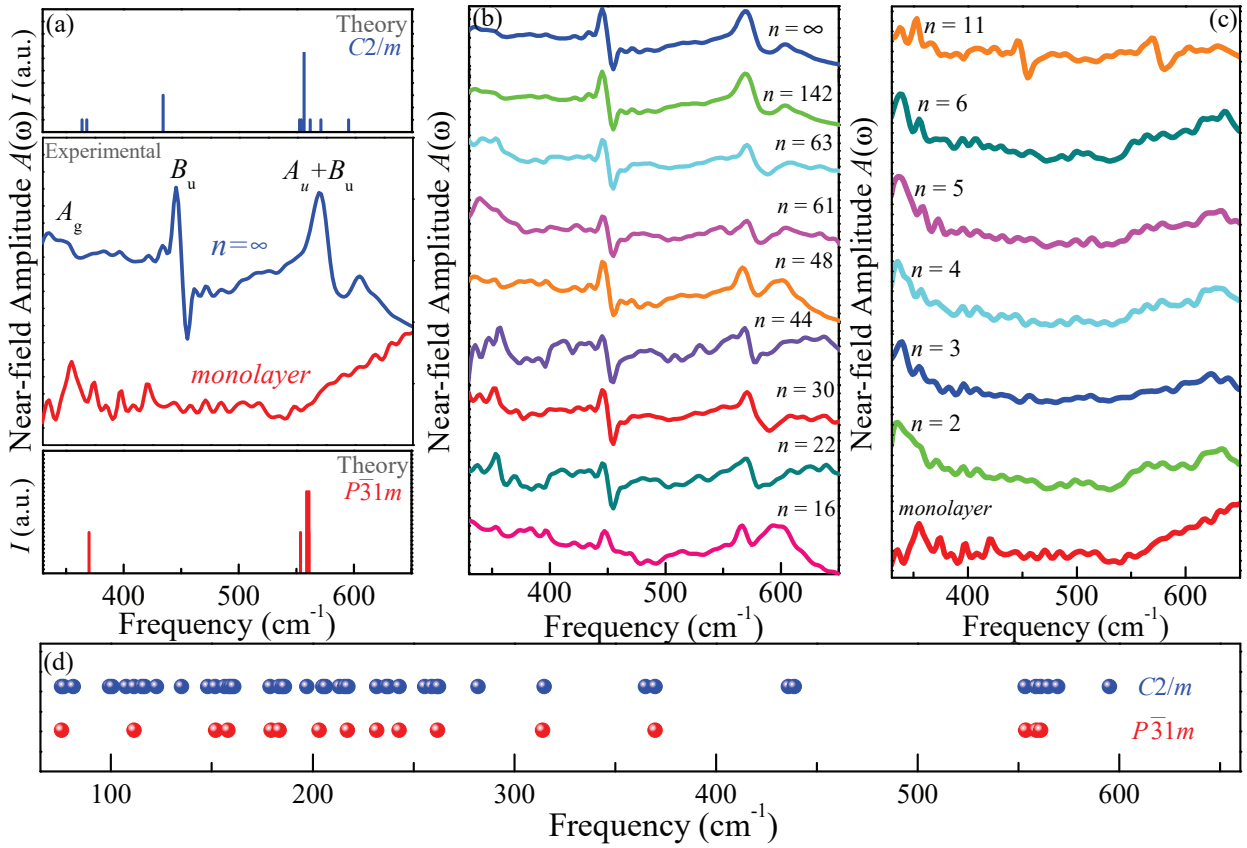

Figure 3: *(a) Near-field infrared response of $MnPS_3$ single crystal compared with that of the monolayer. Corresponding lattice dynamics calculations highlight the symmetry modifications. We show both the infrared- and Raman-active modes. (b,c) Evolution of the near-field infrared spectra from $MnPS_3$ single crystals ($n=\infty$) to the monolayer. The exfoliated sheets are on a gold substrate. In (b) and (c), the spectra are shifted (by a constant amount) for clarity. (d) Direct comparison of the predicted vibrational modes over the entire frequency range for a single sheet of $MnPS_3$ - depending on the symmetry that was imposed during the calculation ($C2/m$ vs.$P\bar{3}1m$).*

feature is at the limit of our sensitivity in the bulk, becomes somewhat more apparent in the intermediate thickness range, and is fairly clear in the n=11 spectrum. The trends are less obvious in few layer systems except the A_g mode (now actually A_{1g}[46]) which appears clearly and is even amplified in the monolayer spectrum. The A_u + B_u sulfur-phosphorous stretching modes near 556 cm^{-1} also display signatures of a thickness-dependent symmetry transition. This feature is strong and fairly wide in the bulk - as expected when a number of closely-related modes overlap. The structure evolves with decreasing thickness sporting a clear doublet between n=142 and 48. The low frequency branch of the doublet redshifts

with decreasing thickness whereas the high frequency branch blueshifts slightly. The doublet broadens significantly between $n = 44$ and 22. Between n=16 and 11, the two branches come together somewhat and begin to diminish. Below n=11, the features are much more diffuse and eventually (n=1) overcome by the gold$\cdots$sulfur charge transfer band above 550 cm^{-1}.[44] A combined analysis of the near-field spectra and lattice dynamics calculations substantiate the connection between decreasing layer number and a crossover to higher symmetry.

It is curious that three-fold symmetry is restored below $n = 11$ rather than at $n = 1$ where the stacking becomes irrelevant. We speculate that, since interactions between adjacent layers in this wide-gap (≈2.65 eV) semiconductor are weak,[47] thermal excitations may restore the higher symmetry below a critical thickness - especially at room temperature. Additional questions relate to stabilizing crystal structures with different stacking symmetries for distinct physical properties in these layered systems as a function of layer thickness or alternate growth conditions. This is important because certain stacking patterns may give rise to distinct magnetic order or even complex order parameters such as ferrotoroidicity.[34] In this regard, synchrotron-based near-field spectroscopy will become a crucial tool for exploring few-layer van der Waals compounds and ultrathin oxide heterostructures.

Conclusion

Synchrotron-based near-field infrared spectroscopy provides a unique platform for evaluating complex chalcogenides like $MnPS_3$. As discussed in detail throughout the text, this technique is a fusion of a high brightness source, Fourier transform techniques, and a tip to localize the radiation. To complement this revolutionary spectroscopic approach, we also developed a general method for stabilizing complex chalcogenides in few- and single-sheet form onto a bare gold substrate. That method is outlined here and then utilized to reveal the dynamics of our target material $MnPS_3$ in few- and single layer form. Traditional infrared absorption and Raman scattering as well as complementary first principles lattice dynamics calcula-

tions supported this effort. Near-field measurements reveal a dramatic change in spectral characteristics under confinement. Perhaps the most striking trend involves the B_u mode near 450 cm^{-1} which disappears almost completely in the thinnest sheets. Combined with the amplified response of the A_g mode and analysis of the A_u + B_u features, we find that symmetry is unexpectedly increased, rather than decreased, in monolayer $MnPS_3$. The monoclinicity of this system is thus a consequence of long-range stacking patterns rather than the local structure. One test of this supposition is how the symmetry crossover changes in the $MnPS_3$, $NiPS_3$, and $FePS_3$ series - a subject of future work. Near-field infrared spectroscopy therefore has the potential to unlock a much wider field of investigation into the properties of atomically-thin materials.

Methods

Single crystals of $MnPS_3$ were prepared via chemical vapor transport as described previously.[48] Surface-exfoliated crystals were mounted on pin-hole apertures for both infrared and Raman measurements. Traditional far-field infrared studies were performed on a Bruker IFS 113v Fourier-infrared spectrometer equipped with a bolometer detector over the 20-700 cm^{-1} frequency range with resolution of 2 cm^{-1}. The measured transmittance was converted to absorption as $\alpha(\omega)$= -$\frac{1}{d}$ln($\mathcal{T}(\omega)$), where $\mathcal{T}(\omega)$ is measured transmittance and d is thickness. No attempt was made to do a reflectance correction to the transmittance. Raman scattering was performed on a LabRAM HR Evolution Raman spectrometer (50-700 cm^{-1}) using an excitation wavelength of 532 nm at a power of 0.5 mW with an 1800 line/mm grating.

Synchrotron-based near-field infrared spectroscopy was performed using a commercial nanoscope (neaSNOM, Neaspec GmbH) using the setup at beamline 2.4 at the Advanced Light Source at Lawrence Berkeley National Laboratory.[23] Both amplitude and phase data were collected over the 330-700 cm^{-1} frequency range. A Ge:Cu detector equipped with

2 MHz, low-noise preamplifier, a KRS-5 beamsplitter, and a nitrogen enclosure enabled extension to the far infrared. Prior to the near-field work, single crystals were mechanically exfoliated with thermal release tape and applied to a substrate. As discussed in the text, we tested a number of candidate substrates before selecting an uncoated gold mirror. The sample + substrate are scanned with atomic force microscopy (AFM), first taking a low resolution image to locate possible regions of interest. Once a promising area is confirmed, a high resolution AFM image is used to reveal the full topography. This information is used to (i) confirm cleanliness, (ii) extract a height profile, and (iii) designate areas to measure. Since AFM and near-field infrared operate in the same field of view, we could pinpoint exactly where to collect spectra. Repeated measurements over several hours confirmed that the sheets are stable. Sheet thickness was calculated using $xm + yn = H$, where H is the extracted height (nm), x is the sheet thickness (nm), y is the van der Waal gap thickness, m is the number of sheets, and n is the number of van der Waal layers present which is defined as $n = (m - 1)$. Specifically for $MnPS_3$ $x = 0.322$ nm and $y = 0.327$ nm. The height profile (H) was extracted using the open source software Gwyddion, and we employed a standard to check our height calibration.

Ab-initio density functional theory (DFT) calculations were performed employing Vienna ab-initio Simulation Package (VASP), which employs the projector-augmented wave (PAW) basis set.[49,50] 340 eV of plane-wave energy cutoff and 8×6×8 (15×15×1) Monkhorst-Pack k-grid sampling were employed for monoclinic $C2/m$ (single-layer hexagonal $P\bar{3}1m$) crystal structures. For the single-layer calculation in monoclinic symmetry, a 8×6×1 k-grid was employed along with the bulk in-plane lattice parameters a and b.

For the treatment of electron correlations within DFT, a revised Perdew-Burke-Ernzerhof exchange-correlation functional for crystalline solid (PBEsol) was employed,[51] in addition augmented by on-site Coulomb interactions for transition metal d-orbitals within a simplified rotationally-invariant form of DFT + U_{eff} formalism.[52] Structural optimizations employed force criteria below 10^{-4} eV/Å. PHONOPY code interfaced with VASP was employed to cal-

culate the Γ-point phonon modes for each structure.[53]

Acknowledgments

Research at the University of Tennessee (JLM) is supported by the U.S. Department of Energy, Office of Basic Energy Sciences, Materials Science Division under award DE-FG02-01ER45885. Work at Rutgers University is funded by the National Science Foundation DMREF Grant DMR-1629059. DM acknowledges support from the Gordon and Betty Moore Foundations EPiQS Initiative through Grant GBMF4416. Portions of these measurements utilized beamline 2.4 at the Advanced Light Source, which is a DOE Office of Science User Facility operated under contract no. DE-AC02-05CH11231, including the remote user program from NSLS-II under contract DE-SC0012704.

References

(1) Kaul, A. B. Two-dimensional layered materials: Structure, properties, and prospects for device applications. *J. Mater. Res.* **2014**, *29*, 348–361.

(2) Li, X.; Zhu, H. Two-dimensional MoS_2: Properties, preparation, and applications. *J. Mater.* **2015**, *1*, 33–44.

(3) Mak, K. F.; Lee, C.; Hone, J.; Shan, J.; Heinz, T. F. Atomically thin MoS_2: A new direct-gap semiconductor. *Phys. Rev. Lett.* **2010**, *105*, 136805.

(4) Splendiani, A.; Sun, L.; Zhang, Y.; Li, T.; Kim, J.; Chim, C. Y.; Galli, G.; Wang, F. Emerging photoluminescence in monolayer MoS_2. *Nano Lett.* **2010**, *10*, 1271–1275.

(5) Li, H.; Zhang, Q.; Yap, C. C. R.; Tay, B. K.; Edwin, T. H. T.; Olivier, A.; Baillargeat, D. From bulk to monolayer MoS_2: Evolution of Raman scattering. *Adv. Funct. Mater.* **2012**, *22*, 1385–1390.

(6) Xiao, D.; Liu, G. B.; Feng, W.; Xu, X.; Yao, W. Coupled spin and valley physics in monolayers of MoS_2 and other group-VI dichalcogenides. *Phys. Rev. Lett.* **2012**, *108*, 196802.

(7) Jones, A. M.; Yu, H.; Ghimire, N. J.; Wu, S.; Aivazian, G.; Ross, J. S.; Zhao, B.; Yan, J.; Mandrus, D. G.; Xiao, D.; Yao, W.; Xu, X. Optical generation of excitonic valley coherence in monolayer WSe_2. *Nat. Nanotechnol.* **2013**, *8*, 634–638.

(8) Das, S.; Robinson, J. A.; Dubey, M.; Terrones, H.; Terrones, M. Beyond Graphene: Progress in Novel Two-Dimensional Materials and van der Waals Solids. *Annu. Rev. Mater. Res.* **2015**, *45*, 1–27.

(9) Geim, A. K.; MacDonald, A. H. Graphene: Exploring carbon flatland. *Phys. Today* **2007**, *60*, 35–41.

(10) Bhimanapati, G. R. et al. Recent Advances in Two-Dimensional Materials beyond Graphene. *ACS Nano* **2015**, *9*, 11509–11539.

(11) Song, L.; Ci, L.; Lu, H.; Sorokin, P. B.; Jin, C.; Ni, J.; Kvashnin, A. G.; Kvashnin, D. G.; Lou, J.; Yakobson, B. I.; Ajayan, P. M. Large scale growth and characterization of atomic hexagonal boron nitride layers. *Nano Lett.* **2010**, *10*, 3209–3215.

(12) Zheng, W. et al. Patterning two-dimensional chalcogenide crystals of Bi_2Se_3 and In_2Se_3 and efficient photodetectors. *Nat. Commun.* **2015**, *6*, 0–7.

(13) Liu, Y.; Petrovic, C. Three-dimensional magnetic critical behavior in CrI_3. *Phys. Rev. B* **2018**, *97*, 014420.

(14) Kang, S.; Kang, S.; Yu, J. Effect of Coulomb Interactions on the Electronic and Magnetic Properties of Two-Dimensional $CrSiTe_3$ and $CrGeTe_3$ Materials. *J. Electron. Mater.* **2018**, 3–6.

(15) Lin, M. W.; Zhuang, H. L.; Yan, J.; Ward, T. Z.; Puretzky, A. A.; Rouleau, C. M.; Gai, Z.; Liang, L.; Meunier, V.; Sumpter, B. G.; Ganesh, P.; Kent, P. R.; Geohegan, D. B.; Mandrus, D. G.; Xiao, K. Ultrathin nanosheets of $CrSiTe_3$: A semiconducting two-dimensional ferromagnetic material. *J. Mater. Chem. C* **2016**, *4*, 315–322.

(16) Lee, S.; Choi, K. Y.; Lee, S.; Park, B. H.; Park, J. G. Tunneling transport of mono- and few-layers magnetic van der Waals $MnPS_3$. *APL Mater.* **2016**, *4*, 086108.

(17) Long, G.; Zhang, T.; Cai, X.; Hu, J.; Cho, C. W.; Xu, S.; Shen, J.; Wu, Z.; Han, T.; Lin, J.; Wang, J.; Cai, Y.; Lortz, R.; Mao, Z.; Wang, N. Isolation and Characterization of Few-Layer Manganese Thiophosphite. *ACS Nano* **2017**, *11*, 11330–11336.

(18) Lee, J.; Ko, T. Y.; Kim, J. H.; Bark, H.; Kang, B.; Jung, S. G.; Park, T.; Lee, Z.; Ryu, S.; Lee, C. Structural and Optical Properties of Single- and Few-Layer Magnetic Semiconductor $CrPS_4$. *ACS Nano* **2017**, *11*, 10935–10944.

(19) Chen, P.; Xu, X.; Koenigsmann, C.; Santulli, A. C.; Wong, S. S.; Musfeldt, J. L. Size-dependent infrared phonon modes and ferroelectric phase transition in $BiFeO_3$ nanoparticles. *Nano Lett.* **2010**, *10*, 4526–4532.

(20) O'Neal, K. R.; Patete, J. M.; Chen, P.; Holinsworth, B. S.; Smith, J. M.; Lee, N.; Cheong, S. W.; Wong, S. S.; Marques, C.; Aronson, M. C.; Musfeldt, J. L. Size-dependent vibronic coupling in α-Fe2O$_3$. *J. Chem. Phys.* **2014**, *141*, 044710.

(21) Deisenhofer, J.; Leonov, I.; Eremin, M. V.; Kant, C.; Ghigna, P.; Mayr, F.; Iglamov, V. V.; Anisimov, V. I.; Van Der Marel, D. Optical evidence for symmetry changes above the Néel temperature of $KCuF_3$. *Phys. Rev. Lett.* **2008**, *101*, 157406.

(22) Casto, L. D.; Clune, A. J.; Yokosuk, M. O.; Musfeldt, J. L.; Williams, T. J.; Zhuang, H. L.; Lin, M. W.; Xiao, K.; Hennig, R. G.; Sales, B. C.; Yan, J. Q.; Mandrus, D. Strong spin-lattice coupling in $CrSiTe_3$. *APL Mater.* **2015**, *3*, 041515.

(23) Bechtel, H. A.; Muller, E. A.; Olmon, R. L.; Martin, M. C.; Raschke, M. B. Ultrabroadband infrared nanospectroscopic imaging. *Proc. Natl. Acad. Sci.* **2014**, *111*, 7191–7196.

(24) Carr, G. L. Resolution limits for infrared microspectroscopy explored with synchrotron radiation. *Rev. Sci. Instrum.* **2001**, *72*, 1613–1619.

(25) Khatib, O.; Bechtel, H. A.; Martin, M. C.; Raschke, M. B.; Carr, G. L. Far Infrared Synchrotron Near-Field Nanoimaging and Nanospectroscopy. *ACS Photonics* **2018**, *5*, 2773–2779.

(26) Mastel, S.; Govyadinov, A. A.; Maissen, C.; Chuvilin, A.; Berger, A.; Hillenbrand, R. Understanding the Image Contrast of Material Boundaries in IR Nanoscopy Reaching 5 nm Spatial Resolution. *ACS Photonics* **2018**, *5*, 3372–3378.

(27) Pollard, B.; Maia, F. C.; Raschke, M. B.; Freitas, R. O. Infrared Vibrational Nanospectroscopy by Self-Referenced Interferometry. *Nano Lett.* **2016**, *16*, 55–61.

(28) Chen, J.; Badioli, M.; Alonso-González, P.; Thongrattanasiri, S.; Huth, F.; Osmond, J.; Spasenović, M.; Centeno, A.; Pesquera, A.; Godignon, P.; Zurutuza Elorza, A.; Camara, N.; de Abajo, F. J. G.; Hillenbrand, R.; Koppens, F. H. L. Optical nano-imaging of gate-tunable graphene plasmons. *Nature* **2012**, *487*, 77–81.

(29) Brar, V. W.; Jang, M. S.; Sherrott, M.; Kim, S.; Lopez, J. J.; Kim, L. B.; Choi, M.; Atwater, H. Hybrid surface-phonon-plasmon polariton modes in graphene/monolayer h-BN heterostructures. *Nano Lett.* **2014**, *14*, 3876–3880.

(30) Liu, M. et al. Phase transition in bulk single crystals and thin films of VO_2 by nanoscale infrared spectroscopy and imaging. *Phys. Rev. B - Condens. Matter Mater. Phys.* **2015**, *91*, 245155.

(31) Lu, X. et al. Nanoimaging of Electronic Heterogeneity in Bi_2Se_3 and Sb_2Te_3 Nanocrystals. *Adv. Electron. Mater.* **2018**, *4*, 1–8.

(32) Kusch, P.; Morquillas Azpiazu, N.; Mueller, N. S.; Mastel, S.; Pascual, J. I.; Hillenbrand, R. Combined Tip-Enhanced Raman Spectroscopy and Scattering-Type Scanning Near-Field Optical Microscopy. *J. Phys. Chem. C* **2018**, *122*, 16274–16280.

(33) Klingen, W.; Ott, R.; Hahn, H. Uber die Darstellung und Eigenschaften von Hexathio und Hexaselenohypodiphosphaten. *ZAAC J. Inorg. Gen. Chem.* **1973**, *396*, 271–278.

(34) Ressouche, E.; Loire, M.; Simonet, V.; Ballou, R.; Stunault, A.; Wildes, A. Magnetoelectric $MnPS_3$ as a candidate for ferrotoroidicity. *Phys. Rev. B - Condens. Matter Mater. Phys.* **2010**, *82*, 100408(R).

(35) Joy, P.A. and Vasudevan, S. Optical-absorption spectra of the layered transition-metal thiophosphates MPS_3 (M=Mn, Fe, and Ni). **1992**, *46*, 5134–5141.

(36) Joy, P. A.; Vasudevan, S. Infrared (700-100 cm $^{-1}$) vibrational spectra of the layered transition metal thiophosphates, MPS_3 (M = Mn, Fe and Ni). *J. Phys. Chem. Solids* **1993**, *54*, 343–348.

(37) Zhang, X.; Qiao, X.-F.; Shi, W.; Wu, J.-B.; Jiang, D.-S.; Tan, P.-H. Phonon and Raman scattering of two-dimensional transition metal dichalcogenides from monolayer to bulk material. *Chem. Soc. Rev.* **2015**, *44*, 2757–2785.

(38) Litvin, D. B. Ferroelectric space groups. *Acta Crystallogr. Sect. A* **1986**, *42*, 44–47.

(39) Hughey, K. D.; Clune, A. J.; Yokosuk, M. O.; Al-Wahish, A.; O'Neal, K. R.; Fan, S.; Abhyankar, N.; Xiang, H.; Li, Z.; Singleton, J.; Dalal, N. S.; Musfeldt, J. L. Phonon mode links ferroicities in multiferroic $[(CH_3)_2NH_2]Mn(HCOO)_3$. *Phys. Rev. B* **2017**, *96*, 180305(R).

(40) Wang, Q.; Zhang, Q.; Zhao, X.; Luo, X.; Wong, C. P. Y.; Wang, J.; Wan, D.; Venkatesan, T.; Pennycook, S. J.; Loh, K. P.; Eda, G.; Wee, A. T. Photoluminescence Upconversion by Defects in Hexagonal Boron Nitride. *Nano Lett.* **2018**, *18*, 6898–6905.

(41) Mathey, Y.; Clement, R.; Sourisseau, C.; Lucazeau, G. Vibrational Study of Layered MPX_3 Compounds and of Some Intercalates with $Co(\eta 5\text{-}C_5H_5)^{2+}$ or $Cr(\eta 6\text{-}C_6H_6)^{2+}$. *Inorg. Chem.* **1980**, *19*, 2773–2779.

(42) Jain, P. K.; Ghosh, D.; Baer, R.; Rabani, E.; Alivisatos, A. P. Near-field manipulation of spectroscopic selection rules on the nanoscale. *Proc. Natl. Acad. Sci.* **2012**, *109*, 8016–8019.

(43) $MnPS_3$ showed poor adhesion on glass and sapphire substrates requiring the use of glue. Bare aluminum and silicon proved to be much better candidates - at least in terms of adhesion. The aluminum substrate allowed for high quality spectra for multilayer samples, however, sharpness of features decreased dramatically with sheet number. This substrate was especially unencouraging because we were unable to get down to the thinnest sheets. Different issues arise with silicon. Although adhesion was reasonable, substrate phonons can potentially overlap with those of the target material. This is especially problematic when the near-field infrared signal is small. For our specific case, the substrate phonons complicate the spectral response of the $MnPS_3$ sheets .

(44) Pensa, E.; Cortés, E.; Corthey, G.; Carro, P.; Vericat, C.; Fonticelli, M. H.; Benítez, G.; Rubert, A. A.; Salvarezza, R. C. The chemistry of the sulfur-gold interface: In search of a unified model. *Acc. Chem. Res.* **2012**, *45*, 1183–1192.

(45) Zhao, X.-M.; Liu, H.-y.; Goncharov, A. F.; Zhao, Z.-W.; Struzhkin, V. V.; Mao, H.-K.; Gavriliuk, A. G.; Chen, X.-J. Pressure effect on the electronic, structural, and vibrational properties of layered 2H-$MoTe_2$. *Phys. Rev. B* **2019**, *99*, 024111.

(46) Ribeiro-Soares, J.; Almeida, R. M.; Barros, E. B.; Araujo, P. T.; Dresselhaus, M. S.; Cançado, L. G.; Jorio, A. Group Theory analysis of phonons in two-dimensional Transition Metal Dichalcogenides. **2014**, *115438*.

(47) Kim, H. S.; Kee, H. Y. Crystal structure and magnetism in α-RuCl3: An ab initio study. *Phys. Rev. B* **2016**, *93*, 155143.

(48) Joy, P. A.; Vasudevan, S. The Intercalation Reaction of Pyridine with Manganese Thiophosphate, $MnPS_3$. *J. Am. Chem. Soc.* **1992**, *114*, 7792–7801.

(49) Kresse, G.; Furthmüller, J. Efficient iterative schemes for ab initio total-energy calculations using plane-wave basis set. *Phys. Rev. B* **1996**, *54*, 11169–11186.

(50) Kresse, G.; Joubert, D. Bridging the THz to RF gap by four-wave mixing in a highly nonlinear fiber. **1999**, *59*, 1758–1775.

(51) Perdew, J. P.; Ruzsinszky, A.; Csonka, G. I.; Vydrov, O. A.; Scuseria, G. E.; Constantin, L. A.; Zhou, X.; Burke, K. Generalized gradient approximation for solids and their surfaces. *Phys. Rev. Lett.* **2008**, *100*, 136406.

(52) Dudarev, S. L.; Botton, G. A.; Savrasov, S. Y.; Humphreys, C. J.; Sutton, A. P. Electron-energy loss spectra and the structural stability of nickel oxide: An LSDA + U study. **1998**, *57*, 1505–1509.

(53) Togo, A.; Tanaka, I. First principles phonon calculations in materials science. *Scr. Mater.* **2015**, *108*, 1–5.